Supporting information

Low-Overpotential and Chloride-Resistant Oxygen Evolution from Alkaline Seawater Enabled by a Synergistic $CeFeNi_4/MnO_2$ Heterostructure

Xue Yang [a], Liangkun Qiu [b, c], Zengfu Wang [b], Longyongxue Ma [b], Xiangjie Chen [b], Sitong Li [a], Jiayi Duan [a], Hongtao Gao [b*]

[a] Hebei Minzu Normal University, Chengde, 067000, China

[b] Key Laboratory of Optic-electric Sensing and Analytical Chemistry for Life Science (Ministry of Education), College of Chemistry and Molecular Engineering, Qingdao University of Science and Technology, Qingdao, 266042, China

[c] Shandong Environmental Protection Development Group Science and Technology Innovation Co., Ltd., Jinan, 250000, China.

*** Corresponding author, E-mail address:** gaohtao@qust.edu.cn **(H. Gao)**

Experimental

Preparation of MnO_2/NF

A piece of nickel foam (NF, 2 × 1.5 cm^2) was first ultrasonicated in 1 M hydrochloric acid (HCl), DI water, and ethanol for 20, 5, and 20 min, respectively. Then the treated NF was removed to a vacuum drying oven at 60 ℃. 1 mmol $KMnO_4$ was dissolved in 30 mL DI water. The clarified solution was transferred to a 50 mL autoclave with the treated NF. The autoclave was sealed and put in the oven, and heated at 120 ℃ for 12 h. After the autoclave cooled down to room temperature, the MnO_2/NF was washed with DI water and ethanol three times, respectively. The obtained MnO_2/NF was stored in a vacuum drying oven.

Preparation of $CeFeNi_4/MnO_2$/NF

The $CeFeNi_4$ was grown on the surface of MnO_2 via electrodeposition. First of all, 1 mmol iron (III) nitrate nonahydrate ($Fe(NO_3)_3·9H_2O$), 2 mmol nickel nitrate hexahydrate ($Ni(NO_3)_2·6H_2O$), 15 mmol Sodium citrate, and 0.3 mmol cerium (III) nitrate hexahydrate ($Ce(NO_3)_3·6H_2O$) were dissolved in 50 mL DI water through stirring to get homogeneous clarified solution. Then, a typical three-electrode system was used for electrodeposition for 30 min under the current density of 50 mA cm^{-2} at 25 ℃, with a piece of MnO_2/NF, a graphite rod, and an Ag/AgCl electrode utilized as the working electrode, counter electrode, and reference electrode, respectively. After washing with DI water and ethanol, the $CeFeNi_4/MnO_2$/NF was removed to a vacuum drying oven at 60 ℃. As the control samples, CeFeNi/NF was prepared by directly electrodeposition on the surface of NF via the same electrodeposition method for $CeFeNi_4/MnO_2$/NF. And the NiFe/MnO_2/NF followed the same process for $CeFeNi_4/MnO_2$/NF, except without $Ce(NO)_3·6H_2O$ added in the electrodeposition solution.

Preparation of alkaline seawater

Seawater was collected from the Zhanqiao Pier in Qingdao, Shandong Province, China. To precipitate the Ca^{2+} and Mg^{2+} effectively, 6.8 g Na_2CO_3 was added to 1000

mL under stirring at room temperature. After Na_2CO_3 reacted with Ca^{2+} and Mg^{2+} completely, a clear solution was obtained by vacuum filtration. Potassium hydroxide (KOH) was dissolved in the collected solution to prepare an alkaline seawater (1M KOH + seawater)[1].

Material characterizations

The X-ray diffraction pattern (XRD, Bruker D8) was applied to characterize phase structures of samples at a scan rate of 10° min^{-1}, ranging from 5° to 90°. A scanning electron microscope (SEM, JSM-6700F) and transmission electron microscope (TEM, JEM-2100PLUS) characterized the morphology and elemental mapping images. The chemical composition was determined by X-ray photoelectron spectroscopy (XPS, Thermo Fisher Scientific K-Alphah). Elemental content was determined using an inductively coupled plasma optical emission spectrometer (ICP-OES, Agilent 720ES).

Theoretical calculations

The CeNi4Fe (001) surface was constructed, and the Ni5Fe model was obtained by first building a Ni (111) slab and subsequently substituting 8 Ni atoms with Fe. Free-energy profiles were obtained using the computational hydrogen electrode (CHE) model. All spin-polarized density functional theory (DFT) calculations were carried out with Vienna Ab initio Simulation Package (VASP) employing the projector augmented-wave (PAW) pseudopotentials[2,3]. The electron–electron exchange and correlation were treated within the generalized gradient approximation of Perdew, Burke, and Ernzerhof (GGA-PBE) functional[4]. A plane-wave energy cutoff of 400 eV was used. Convergence criteria for the electronic and ionic relaxations were set to 1×10−5 eV and 0.03 eV/Å. The Brillouin zone was sampled using a Monkhorst–Pack k-point grid of 3×3×1 for slab calculations.

Electrochemical measurement

All the electrochemical measurements were carried out on a CHI 760D electrochemical workstation at room temperature (298K). The electrochemical performance was tested using a three-electrode system, with the catalyst (1 × 1 cm^2) as the working electrode, a graphite electrode as the counter electrode, and an Hg/HgO

electrode as the reference electrode. 1 M KOH solution and alkaline seawater were used as electrolytes separately. Before conducting the electrochemical test, the reference electrode calibration was not performed under the hydrogen redox conditions in the same electrolyte. Linear sweep voltammetry (LSV) measurements were conducted at a scan rate of 5 mV s^{-1}. Due to the high conductivity of the electrolyte and the small R_s, a 95 % iR-correction was applied to obtain results closer to the true value. As shown in Figure S1, after compensation, the performance of the catalyst more closely approximates the true value. All the measured potential vs. Hg/HgO (pH=14) throughout the experiments were calculated to a reversible hydrogen electrode utilizing equation (1):

$$E_{RHE} = E_{Hg/HgO} + 0.098 + 0.059\ pH \quad (1)$$

Electrochemically active surface area (ECSA) is measured by the equation:

$$ECSA = \frac{C_{dl}}{C_s} \quad (2)$$

Where C_{dl} is the double-layer capacitance, which is calculated in the non-Faradaic region with different scan rates. C_s is the specific capacitance, which typically takes a value of 0.04 mF cm^{-2}.

The electrochemical impedance spectroscopy (EIS) was recorded from 0.01 Hz to 100 kHz with an amplitude of 5 mV under different potentials.

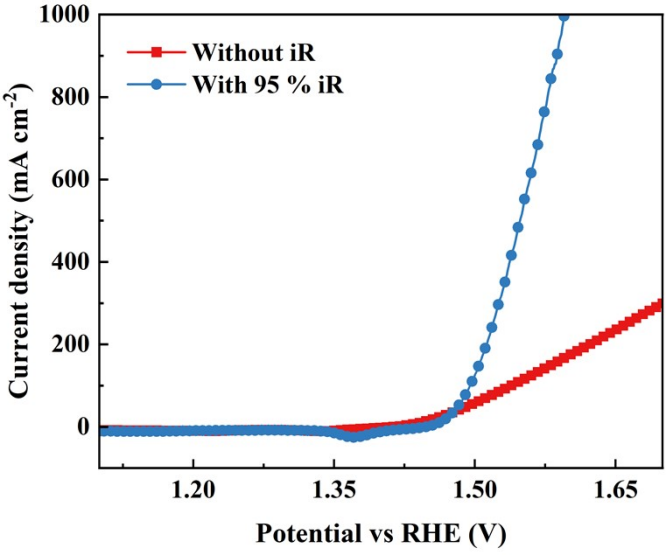

Figure S1. The LSV curves of $CeFeNi_4/MnO_2$/NF with and without iR-correction

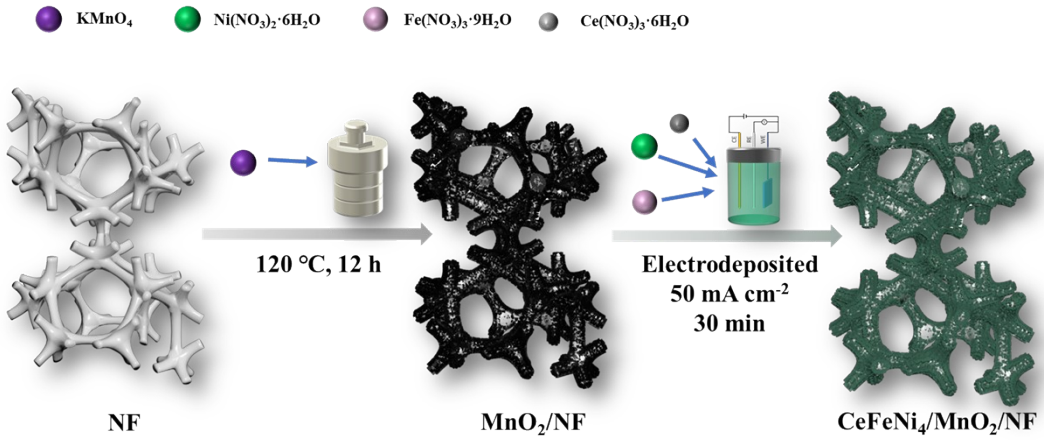

Figure S2. Schematic diagram of the $CeFeNi_4/MnO_2/NF$ electrocatalyst

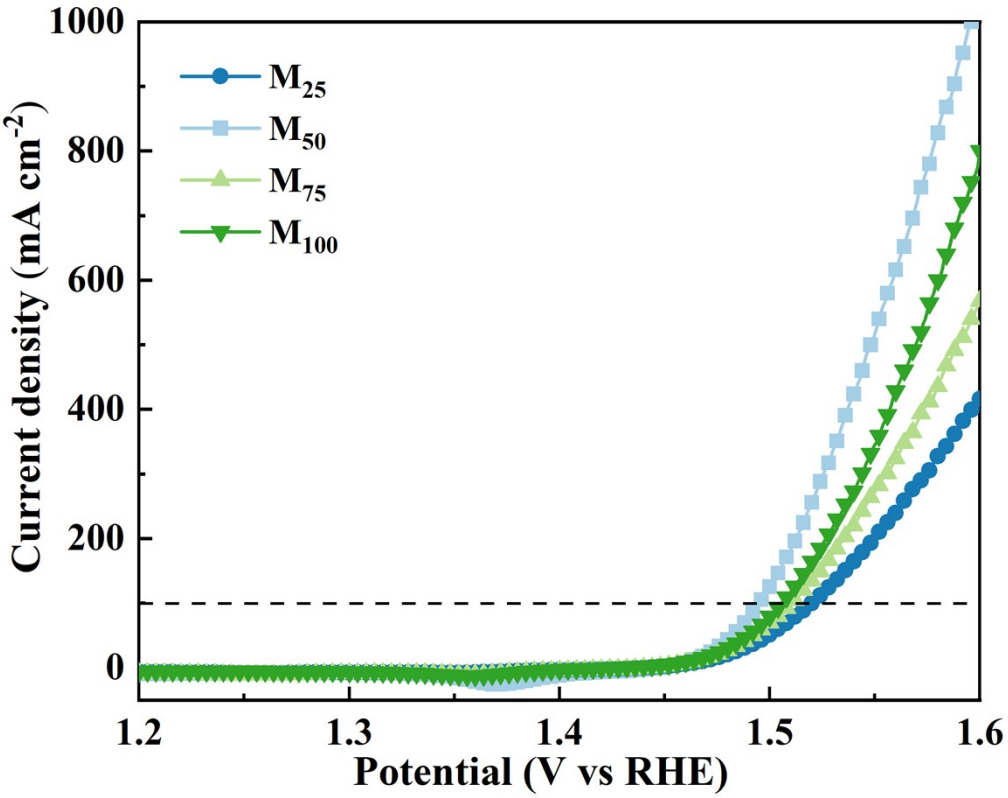

Figure S3. LSVs of M_{25}, M_{50}, M_{75}, and M_{100}.

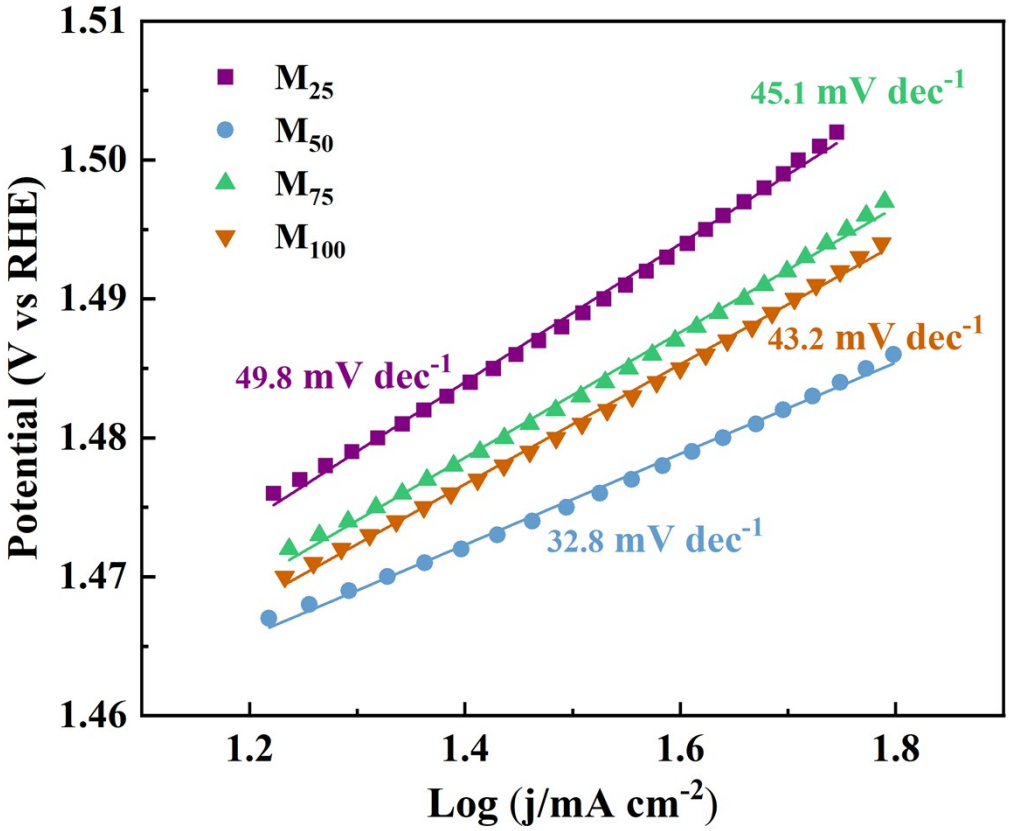

Figure S4. Tafel slope curves of M_{25}, M_{50}, M_{75}, and M_{100}.

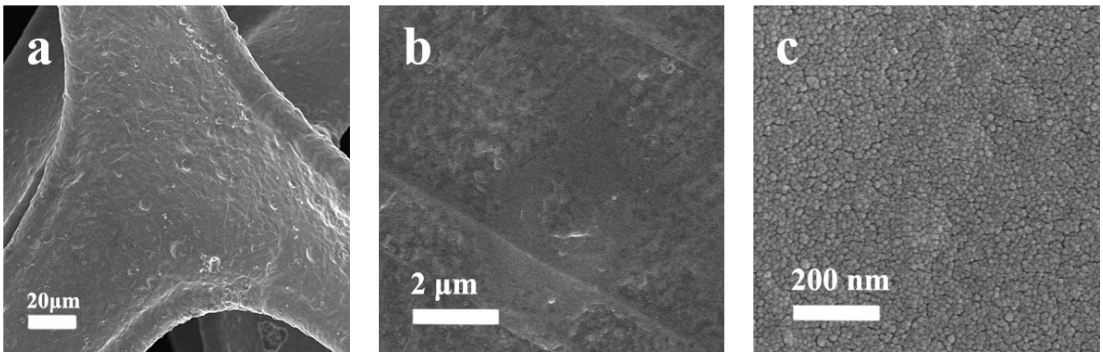

Figure S5. (a - c) SEM images of NF at different magnifications.

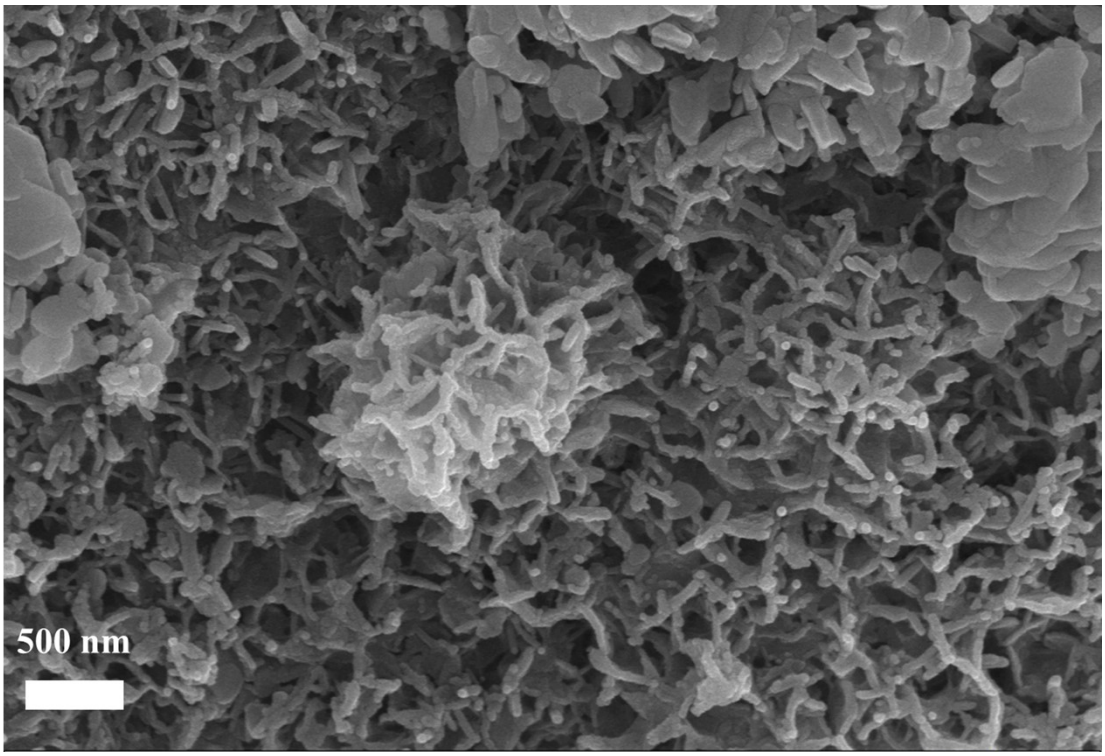

Figure S6. SEM image of MnO_2/NF.

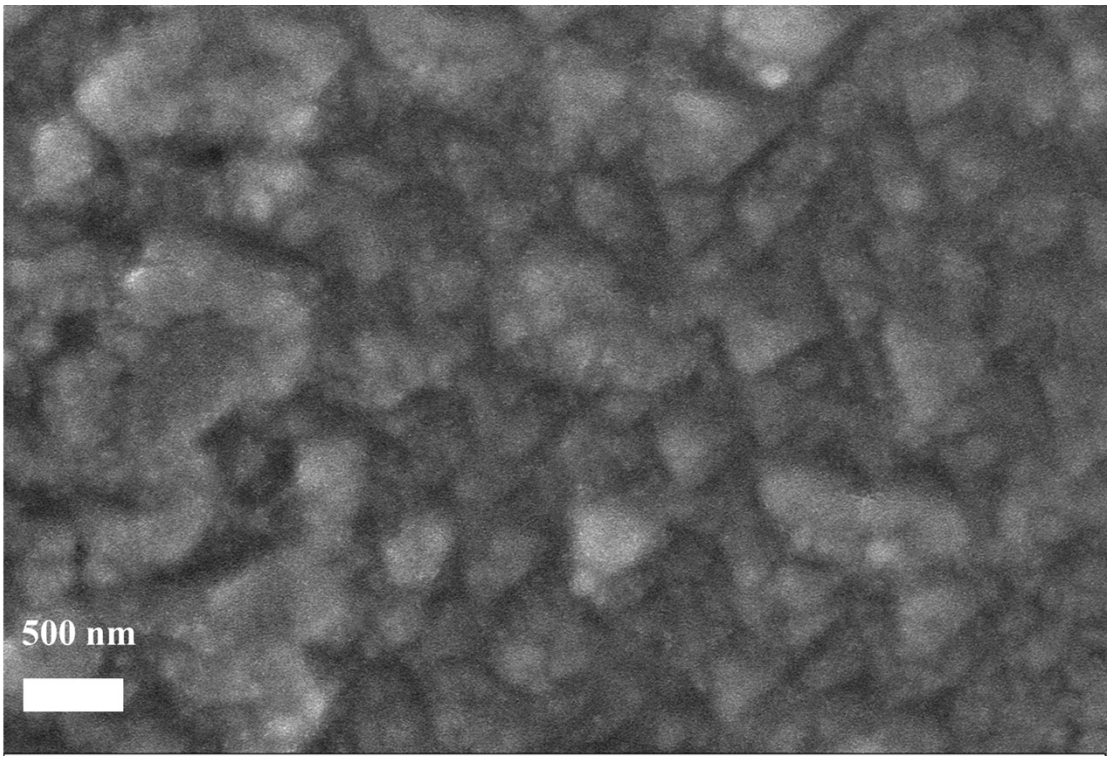

Figure S7. SEM image of CeFeNi/NF.

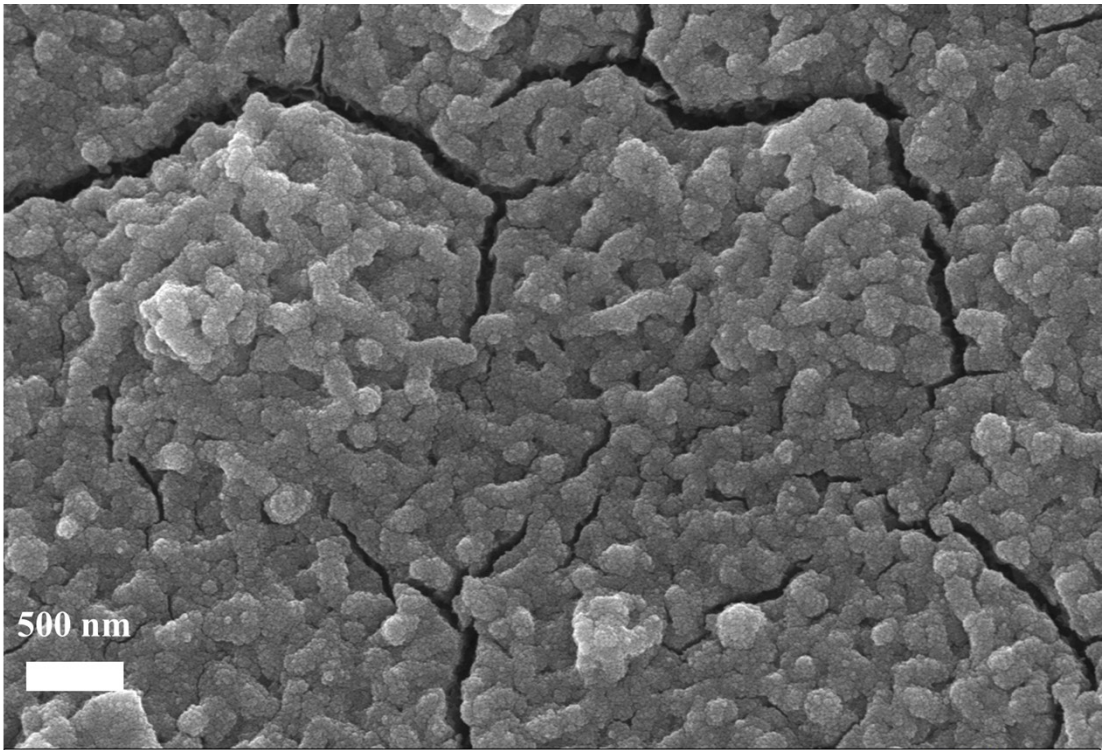

Figure S8. SEM image of $NiFe/MnO_2/NF$.

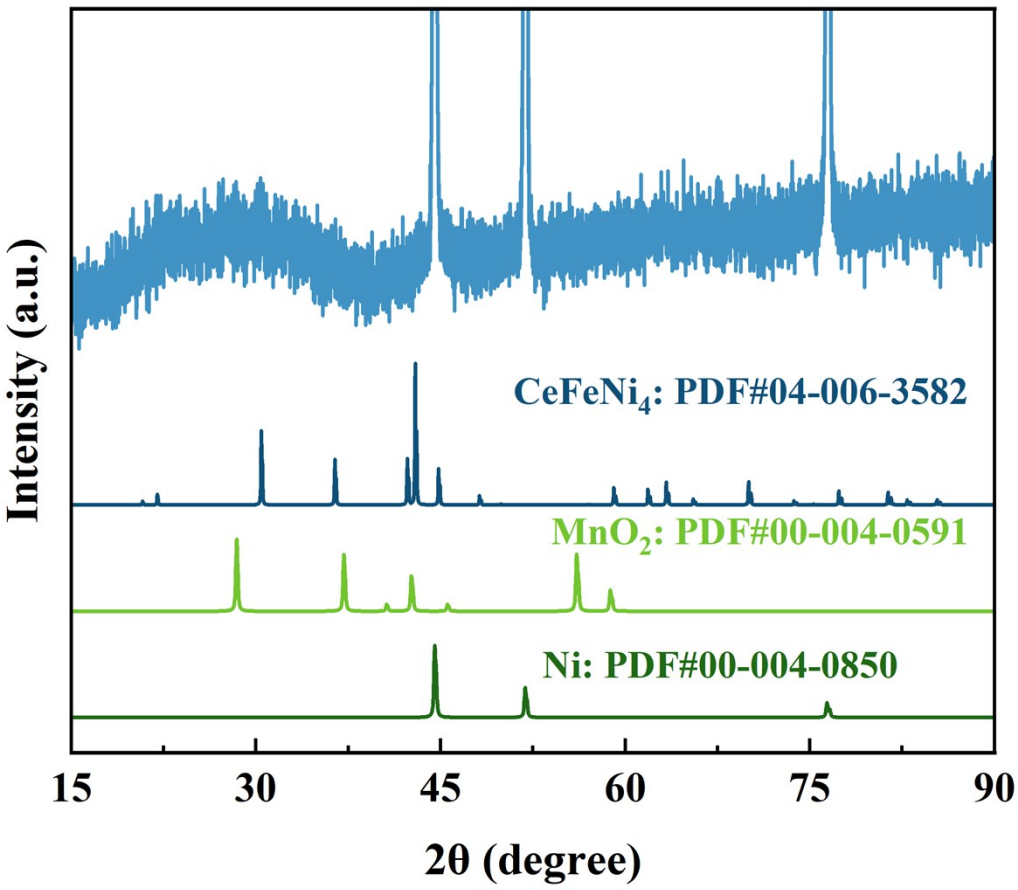

Figure S9. X-ray diffraction (XRD) spectra of $CeFeNi_4/MnO_2$/NF.

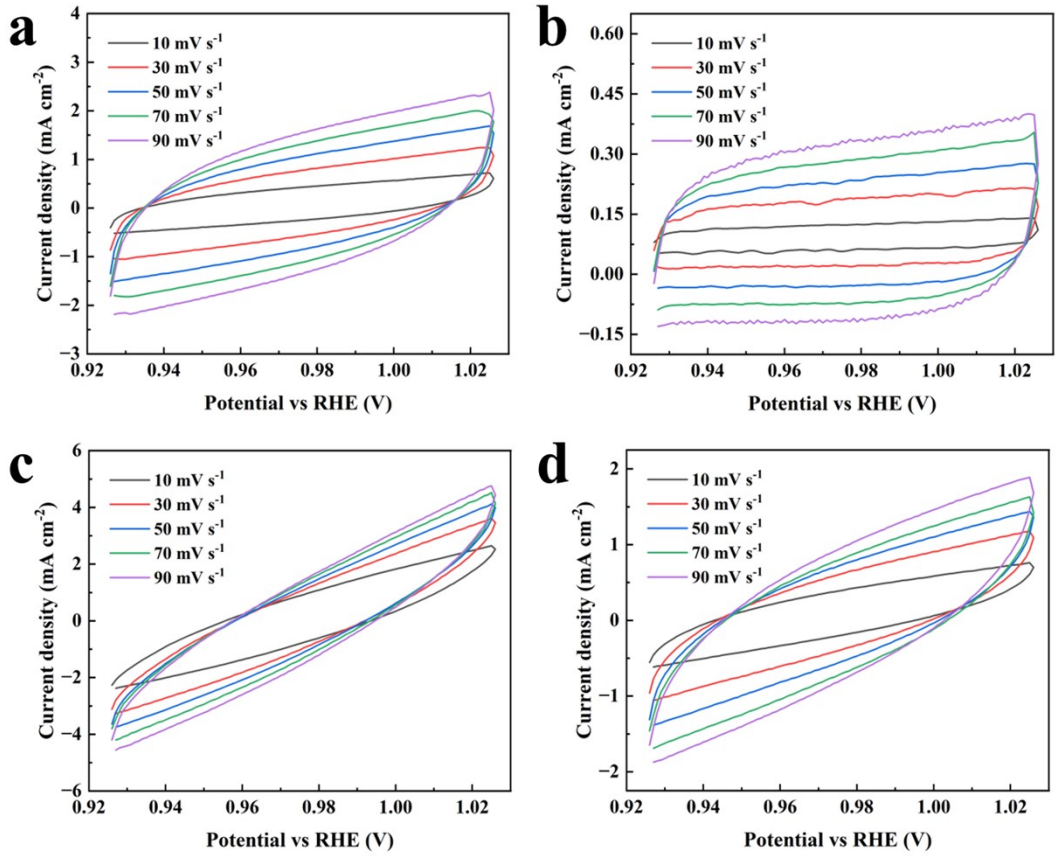

Figure S10. The CV images in the non-Faraday region of (a) $CeFeNi_4/MnO_2/NF$, (b) CeFeNi/NF, (c) $NiFe/MnO_2/NF$, and (d) MnO_2/NF.

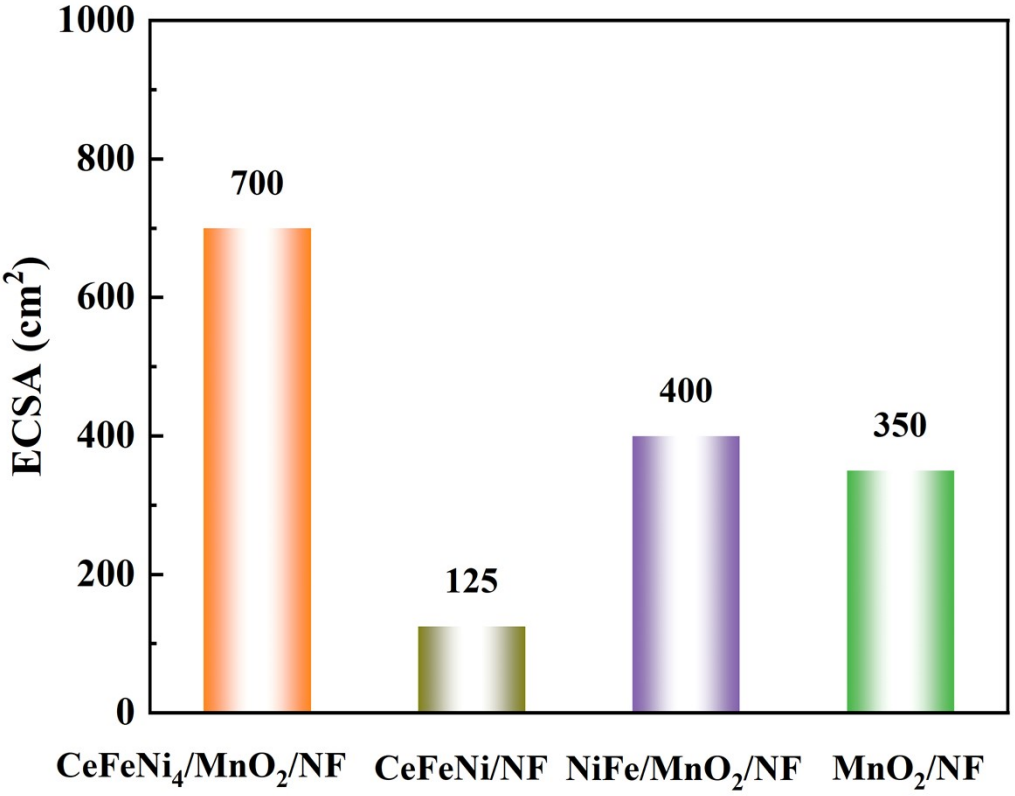

Figure S11. The ECSA values of the as-prepared samples in 1 M KOH solution.

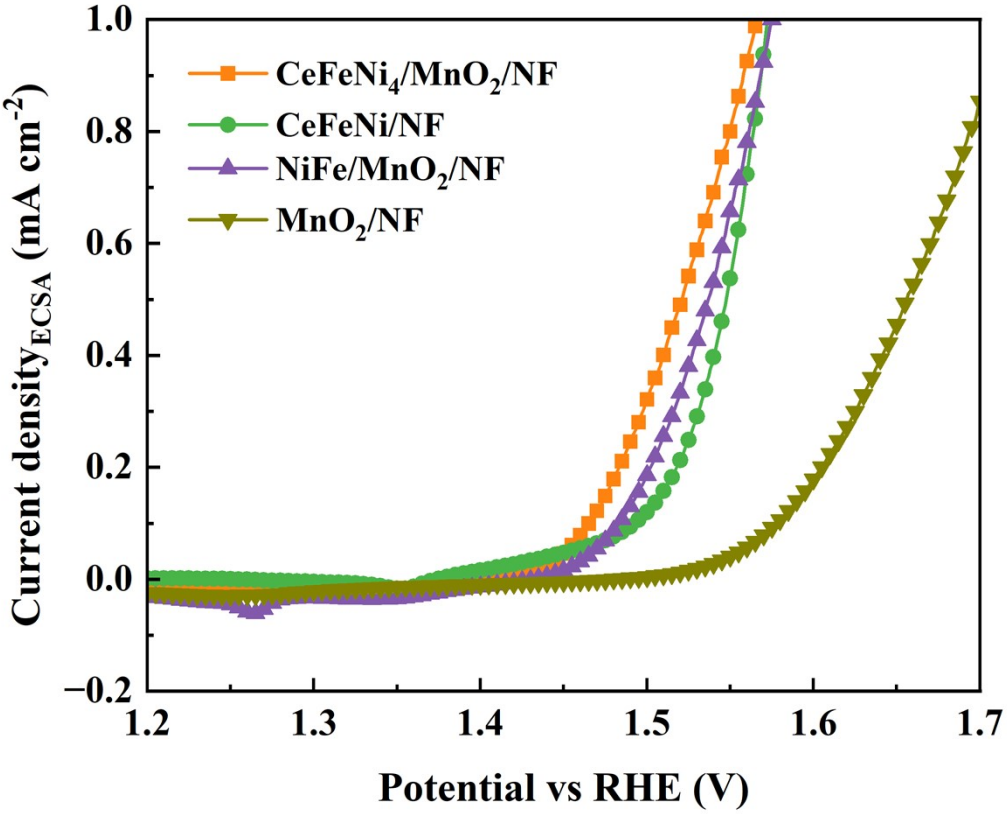

Figure S12. The ECSA normalized LSV curves of $CeFeNi_4/MnO_2/NF$ and the control samples.

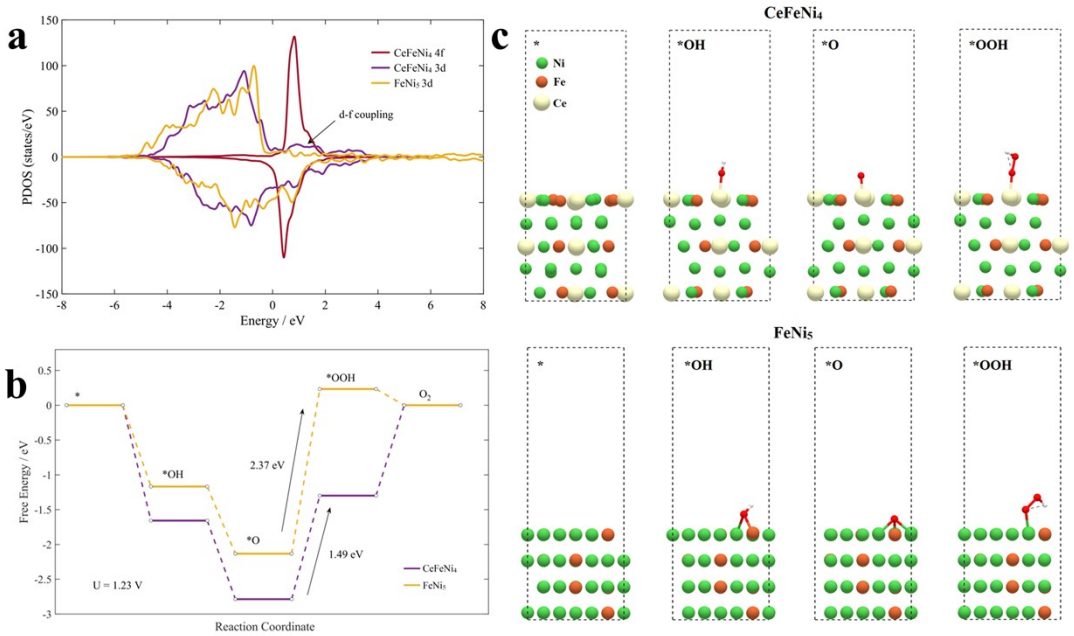

Figure S13. (a) Projected density of states (PDOS) of the 3d and 4f orbitals in $CeFeNi_4$, and the 3d orbitals in Ni_5Fe, (b) Free energy diagram for the oxygen evolution reaction (OER) at 1.23 V for $CeFeNi_4$ and Ni_5Fe, obtained using the computational hydrogen electrode (CHE) model. (c) Intermediate structures of $CeFeNi_4$ and Ni_5Fe during the OER.

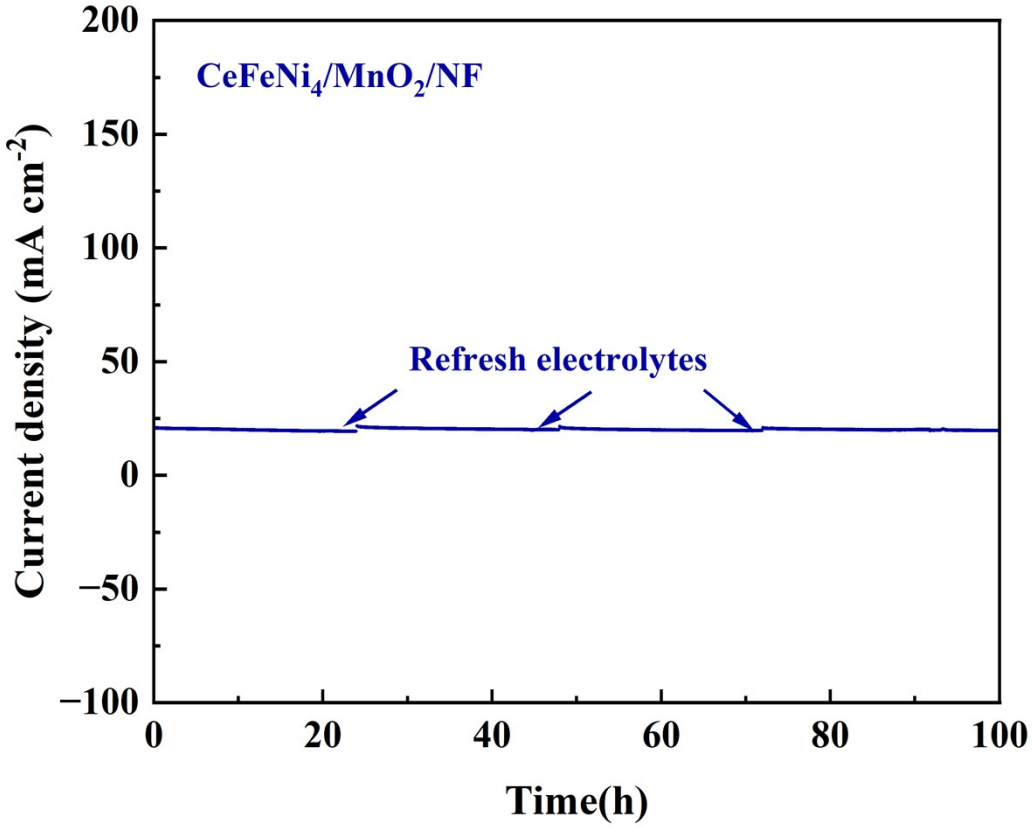

Figure S14. Long-term stability test for $CeFeNi_4/MnO_2$/NF at 20 mA cm^{-2} for 100 h in 1M KOH solution

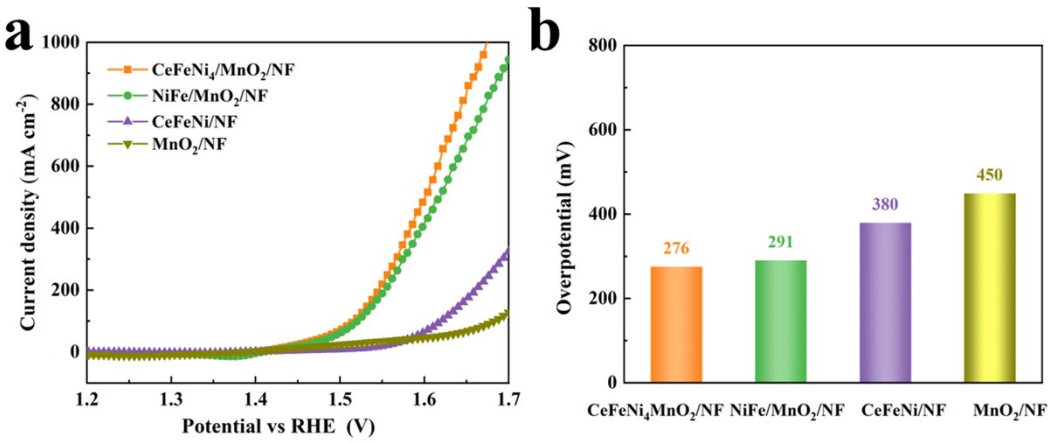

Figure S15. (a) LSV curves and (b) overpotentials at 100 mA cm^{-2} of as-prepared catalysts in alkaline seawater.

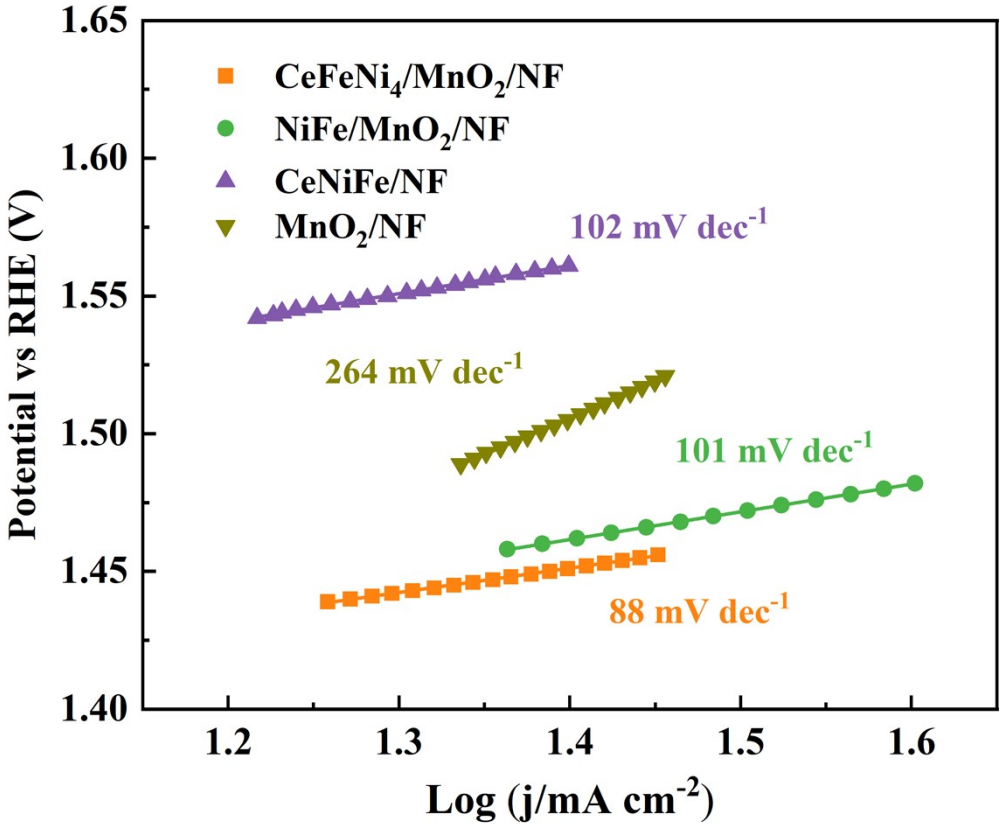

Figure S16. Tafel plots of as-prepared catalysts in alkaline seawater.

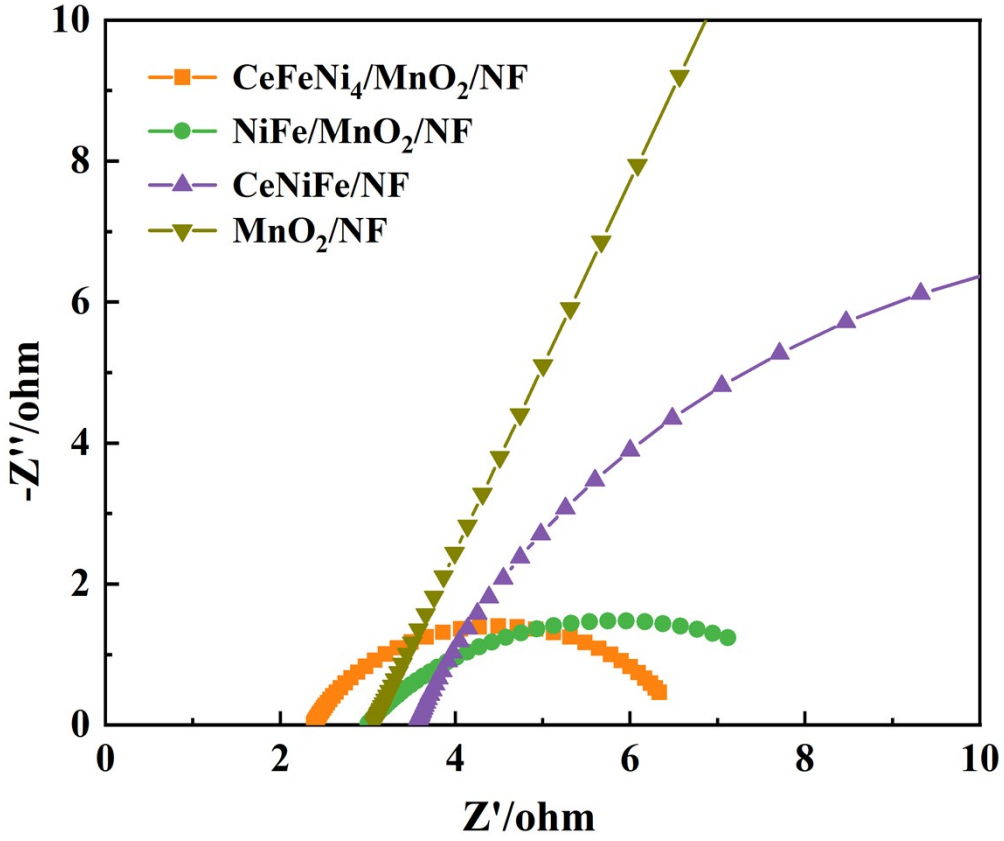

Figure S17. Nyquist plots of as-prepared catalysts in alkaline seawater.

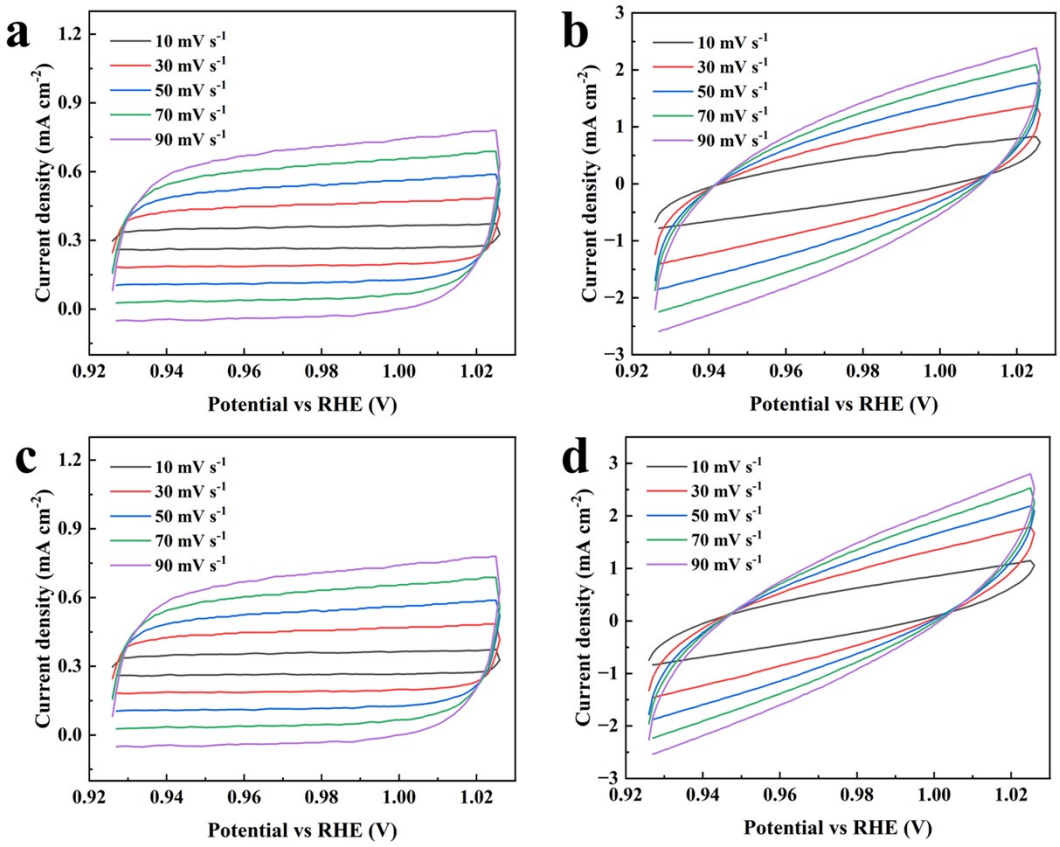

Figure S18. The CV images in the non-Faraday region of (a) $CeFeNi_4/MnO_2/NF$, (b) $NiFe/MnO_2/NF$, (c) CeFeNi/NF, and (d) MnO_2/NF.

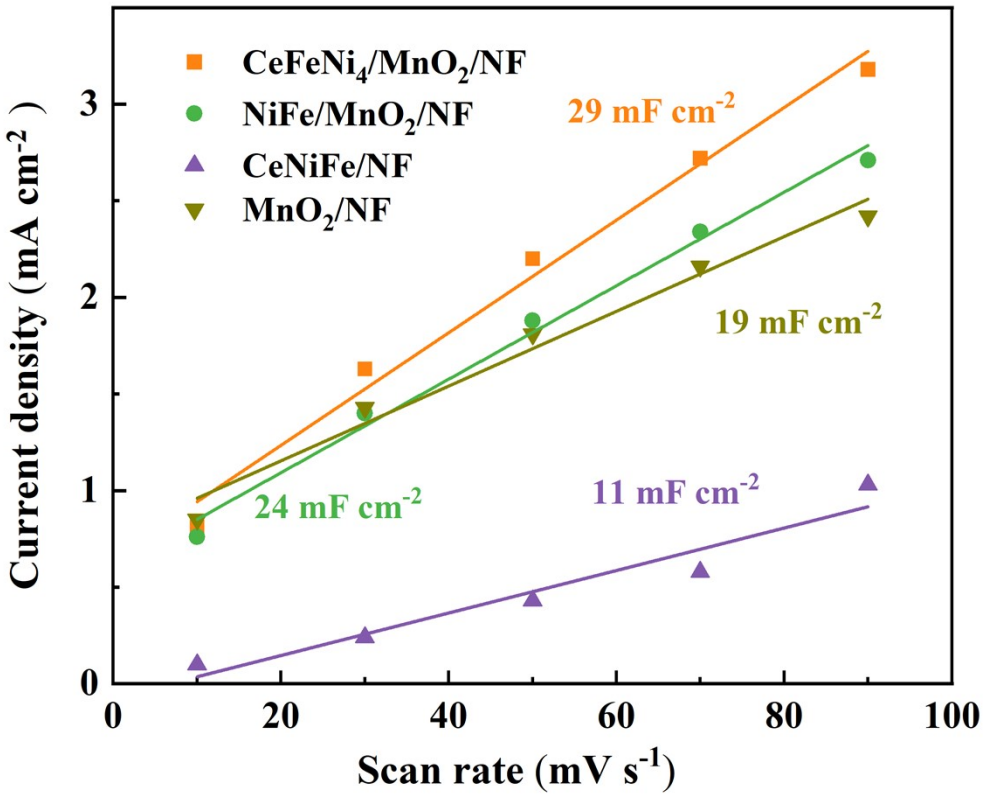

Figure S19. C_{dl} of as-prepared catalysts in alkaline seawater.

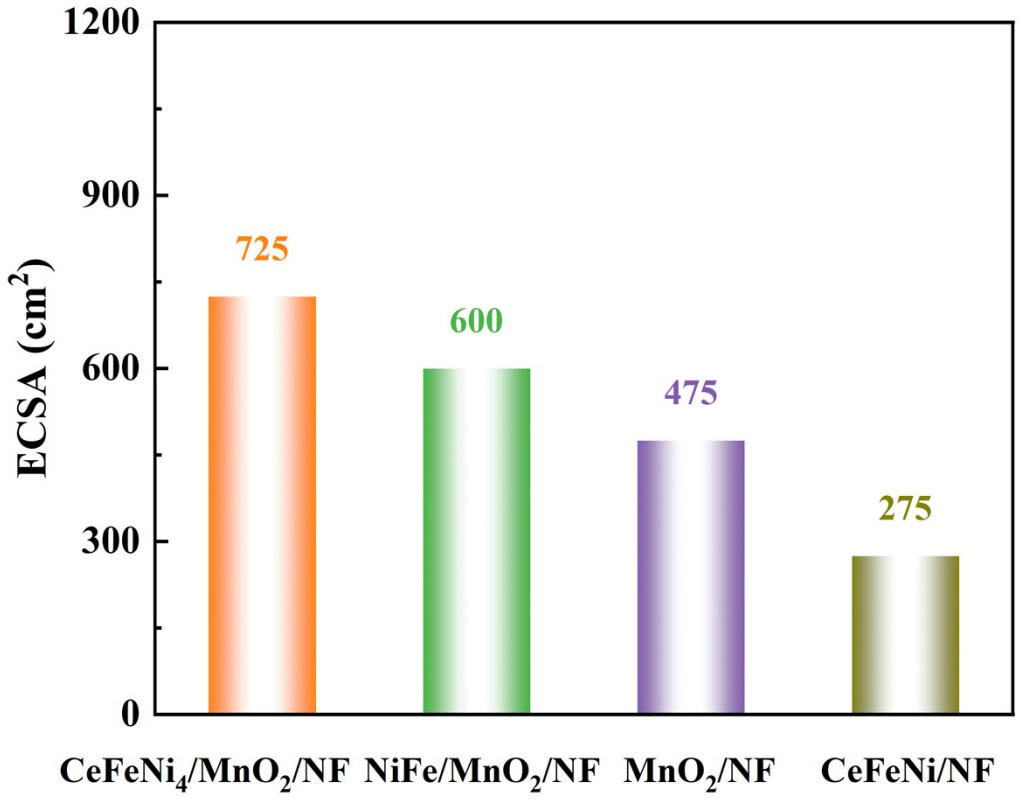

Figure S20. The ECSA values of the as-prepared samples in alkaline seawater.

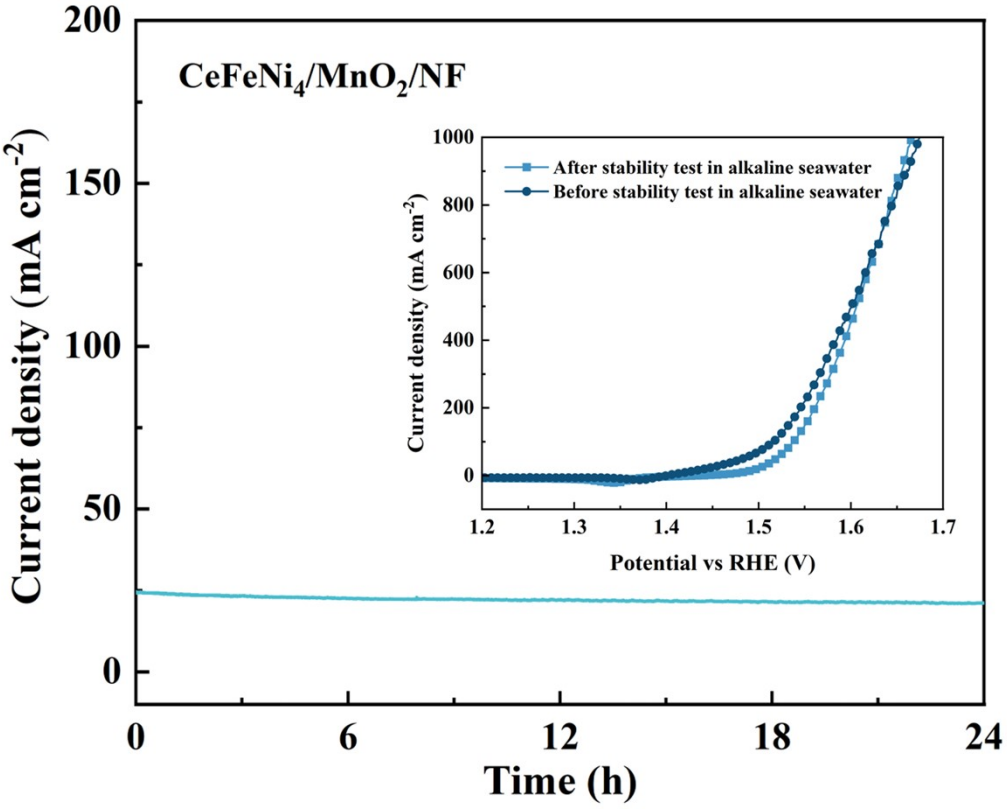

Figure S21. Long-term stability test for $CeFeNi_4/MnO_2/NF$ at 20 mA cm^{-2} for 24 h in alkaline seawater (inset: LSV of $CeFeNi_4/MnO_2/NF$ before and after the stability test).

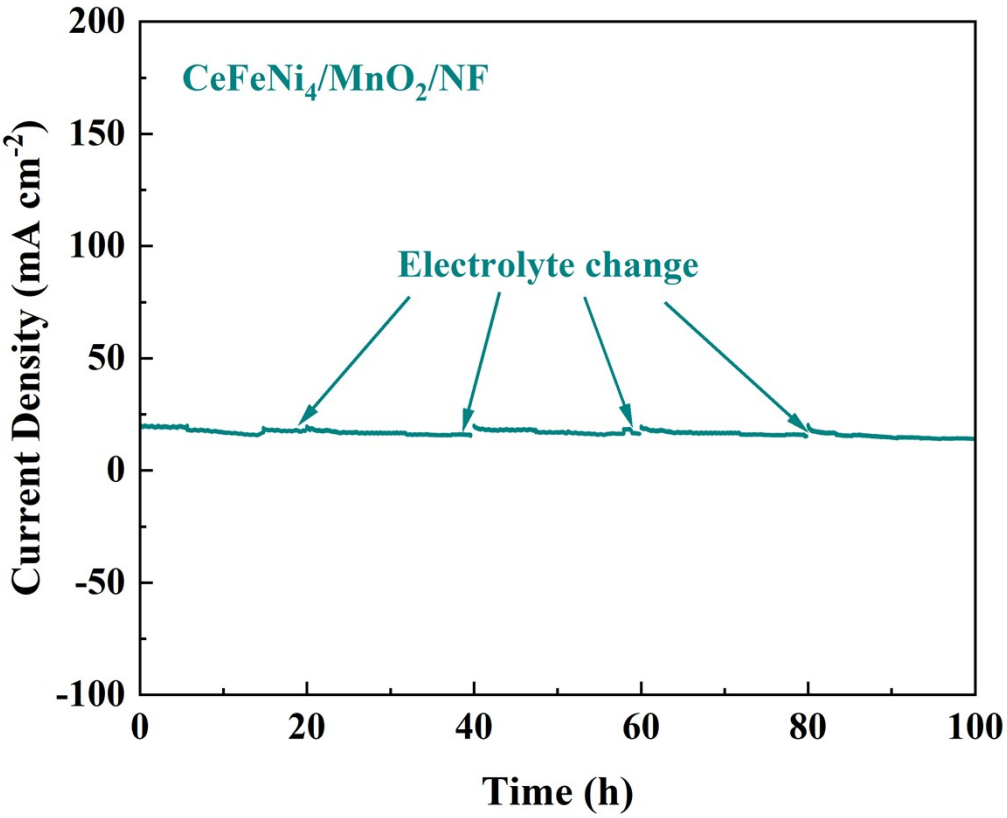

Figure S22. Long-term stability test for $CeFeNi_4/MnO_2$/NF at 20 mA cm^{-2} for 100 h in alkaline seawater.

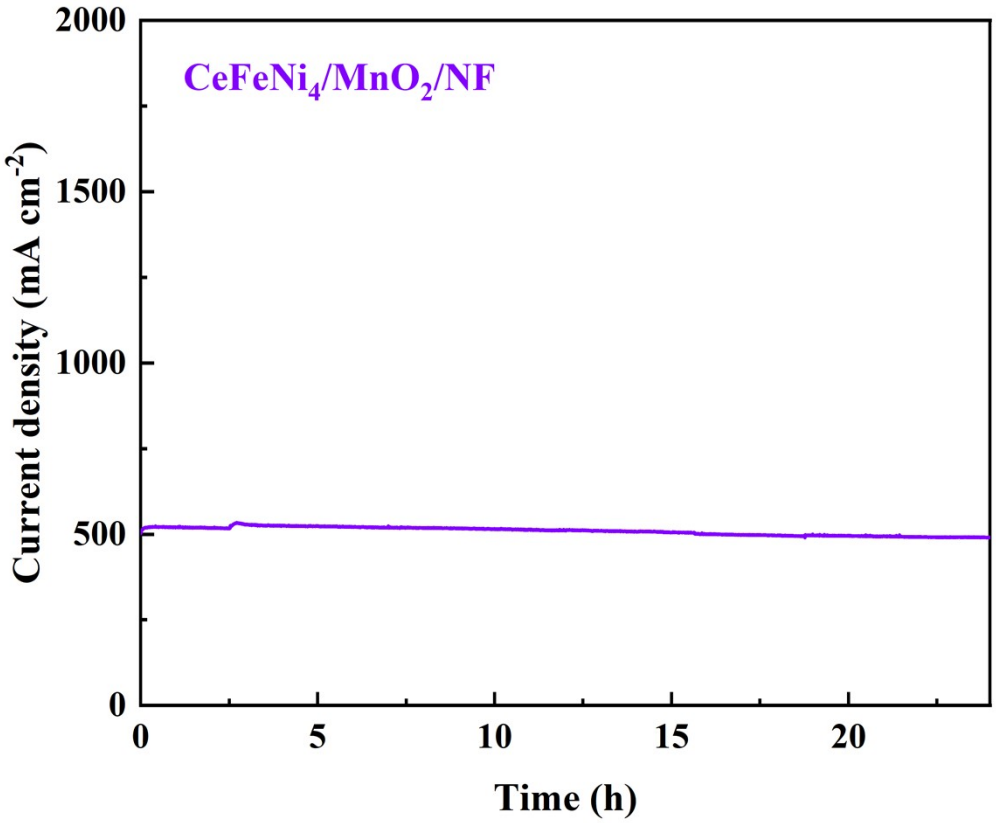

Figure S23. Long-term stability test for $CeFeNi_4/MnO_2$/NF at 500 mA cm^{-2} for 24 h in alkaline seawater.

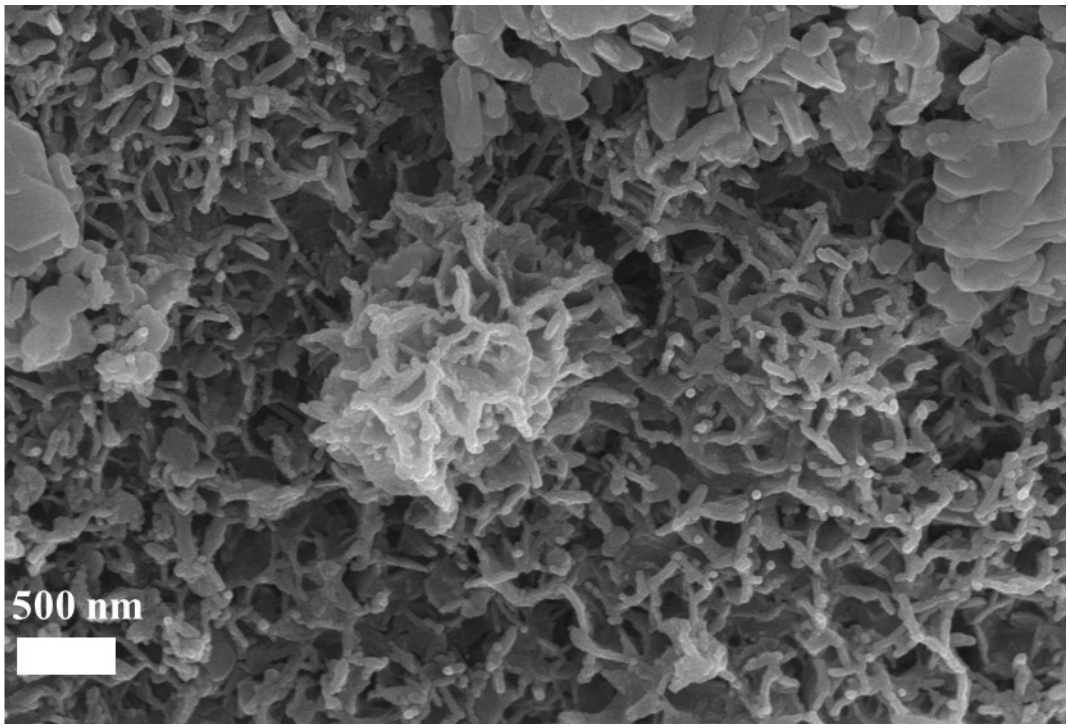

Figure S24. The SEM images of $CeFeNi_4/MnO_2/NF$ after the stability test in the alkaline seawater.

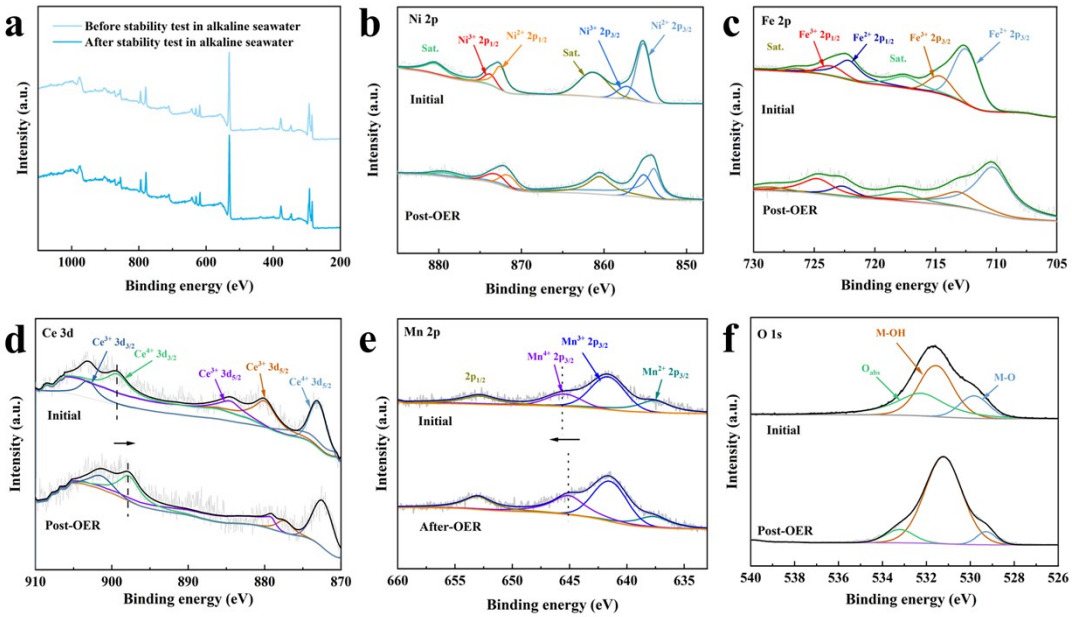

Figure S25. XPS of (a) survey, (b) Ni 2p, (c) Fe 2p, (d) Ce 3d, (e) Mn 2p, and (f) O 1s regions of $CeFeNi_4/MnO_2$/NF before and after the OER stability in alkaline seawater.

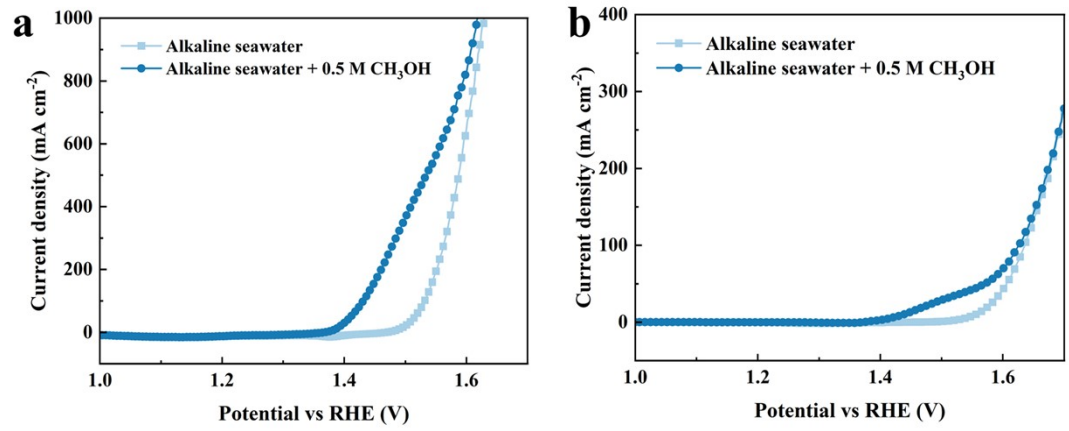

Figure S26the the . LSV curves of $CeFeNi_4/MnO_2$/NF and CeFeNi/NF for OER in alkaline seawater and alkaline seawater + 0.5 M CH_3OH.

Table S1 Comparison of the OER activities of $CeFeNi_4/MnO_2/NF$ with recently reported electrocatalysts in the alkaline seawater or simulated seawater.

Electrocatalysts	Electrolyte	Overpotentials/mV		References
		100 mA cm^{-2}	10 mA cm^{-2}	
$CeFeNi_4/MnO_2/NF$	Alkaline seawater	244	204	this work
Ce–$NiSe_2$/CoP	Simulated seawater	304	440	5
CeO_2/D-NiFe-LDH@Cuw	Alkaline seawater	/	230	6
MnO_2-NiFe-LDH/CC	Alkaline seawater	~270	363	7
Ni-Fe-Ce-B/MS	Simulated seawater	208	297	8
$Ni(OH)_2@CeO_2/NF$	Alkaline seawater	240	374	9
a-NiCoS/c-CeO_x	Simulated seawater	256	/	10
$CeO_2Co_{2-x}Ni_xP@C$	Alkaline seawater	323	/	11
NiFeO-CeO_2/NF	Alkaline seawater	/	270	12
CeO_{2-x}@CoFe-LDH/NF	Alkaline seawater	/	204	13

Table S2 Elemental concentrations in electrolyte solutions before and after stability testing

Element	Concentration/ μg L^{-1}	
	Before the stability test	After the stability test
Ce	0.5	0.7
Mn	16.9	24.6
Ni	9.0	10.1
Fe	130.2	175.5

Table S3. The percentage of Ni^{3+} and Fe^{3+} before and after the stability in alkaline seawater.

	Percentage/%	
	Initial	Post-OER
Ni^{3+}	18	23
Fe^{3+}	28	35

Table S4. The percentage of M-OH before and after the stability in alkaline seawater.

	Percentage/%	
	Initial	Post-OER
M-OH	47	67

References

1. P. Ding, H. Song, J. Chang, and S. Lu, Nano Res., 2022, 15(8), 7063-7070.
2. G. Kresse and J. Furthmüller, Efficient iterative schemes for ab initio total-energy calculations using a plane-wave basis set. Physical Review B 1996, 54, 11169-11186.
3. G. Kresse and J. Furthmüller, Efficiency of ab-initio total energy calculations for metals and semiconductors using a plane-wave basis set. Computational Materials Science 1996, 6, 15-50.
4. J. Perdew, K. Burke, and M. Ernzerhof, Generalized Gradient Approximation Made Simple. Physical Review Letters 1996, 77, 3865-3868.
5. W. Jiang, B. Zhao, Z. Li, P. Zhou, Y. Zhao, X. Chen, J. Wang, R. Yang, and C. Zuo, Int. J. Hydrog. Energy, 2024, 73, 590-597.
6. Z. Wang, L. Wang, L. Chu, M. Yang, and G. Wang, ACS Sustain. Chem. Eng., 2024, 12(31), 11628-11637.
7. F. Liu, M. Fan, H. Yan, Z. Wang, J. Song, H. Wang, and J. Ren, Catalysts, 14(8) 502.
8. H. Liu, X. Zhou, C. Ye, M. Ye, and J. Shen, Appl. Catal. B-Environ., 2024, 343, 123560.
9. C. Lyu, J. Cheng, H. Wang, Y. Yang, K. Song, W. Lau, J. Zheng, X. Zhu, and H. Yang, Adv. Compos. Hybrid Mater., 2023, 6(5), 175.
10. H. Zhang, Y. Gao, J. Li, J. Sun, D. Wang, L. Wang, and Y. Meng, Fuel, 2024, 375, 132652.
11. B. Fang, X. Chu, X. Han, J. He, B. Geng, L. Jia, X. Wang, S. Song, and H. Zhang, Chem. Commun., 2022, 58(99), 13803-13806.
12. H. Zhang, Z. Bi, P. Sun, A. Chen, T. Wågberg, X. Hu, X. Liu, L. Jiang, and G. Hu, ACS Nano, 2023, 17(16), 16008-16019.
13. Y. Hu, W. Liu, K. Jiang, L. Xu, M. Guan, J. Bao, H. Ji, and H. Li, Inorg. Chem. Front., 2020, 7(22), 4461-4468.